Valence instability in the bulk and at the surface of the antiferromagnet $SmRh_2Si_2$

A. Chikina,[1] A. Generalov,[2] K. Kummer,[3] M. Güttler,[1] V. N. Antonov,[4] Yu. Kucherenko,[4] K. Kliemt,[5] C. Krellner,[5] S. Danzenbächer,[1] T. Kim,[6] P. Dudin,[6] C. Geibel,[7] C. Laubschat,[1] and D. V. Vyalikh[8,9,10]

[1]*Institut für Festkörperphysik, Technische Universität Dresden, D-01062 Dresden, Germany*

[2]*MAX IV Laboratory, Lund University, Box 118, SE-22100 Lund, Sweden*

[3]*European Synchrotron Radiation Facility, 71 Avenue des Martyrs, Grenoble, France*

[4]*Institute for Metal Physics, National Academy of Sciences of Ukraine, UA-03142 Kiev, Ukraine*

[5]*Kristall- und Materiallabor, Physikalisches Institut, Goethe-Universität Frankfurt, Max-von-Laue Straße 1, D-60438 Frankfurt am Main, Germany*

[6]*Diamond Light Source, Didcot OX11 0DE, United Kingdom*

[7]*Max-Planck-Institut für Chemische Physik fester Stoffe, D-01187 Dresden, Germany*

[8]*Saint Petersburg State University, Physics Department, Saint Petersburg 198504, Russia*

[9]*Donostia International Physics Center, Departamento de Fisica de Materiales and CFM-MPC UPV/EHU, 20080 San Sebastian, Spain*

[10]*IKERBASQUE, Basque Foundation for Science, 48011 Bilbao, Spain*

(Received 2 February 2017; revised manuscript received 20 March 2017; published 17 April 2017)

Using resonant angle-resolved photoemission spectroscopy and electron band-structure calculations, we explore the electronic structure and properties of Sm atoms at the surface and in the bulk of the antiferromagnet $SmRh_2Si_2$. We show that the Sm atoms reveal weak mixed-valent behavior both in the bulk and at the surface. Although trivalent $4f$ emission strongly dominates, a small divalent $4f$ signal near the Fermi energy can be clearly resolved for surface and bulk Sm atoms. This behavior is quite different to most other Sm-based materials which typically experience a surface valence transition to a divalent state of Sm atoms at the surface. This phenomenon is explained in analogy to the isostructural Ce compound, where strong $4f$ hybridization stabilizes mixed-valent ground state both in the bulk and at the surface, and which were described in the light of the single-impurity Anderson model. Implications for other $RERh_2Si_2$ (RE = rare-earth elements) compounds are discussed.

DOI: 10.1103/PhysRevB.95.155127

I. INTRODUCTION

Among the other rare-earth (RE) intermetallic materials, Sm-based systems are rather unexplored, albeit showing a plenty of exotic low-temperature properties stemming from the interplay between localized $4f$ and itinerant valence electrons. The recent proposition that the canonical Kondo insulator SmB_6 [1–3] exhibits a topological Kondo insulating state [4–9] renews the attention of the community [10] not only in rare-earth hexaborides [11], but also in the Sm-based systems in general [12]. Here, we study the electronic structure of the antiferromagnet (AFM) $SmRh_2Si_2$ ($T_N = 62$ K) [13] by means of resonant angle-resolved photoemission spectroscopy (ARPES), analyzing and comparing the respective data with the results of electron band-structure calculations and predictions from a simple thermochemical model.

A particular feature of $RERh_2Si_2$-type materials is that their structure is characterized by two-dimensional layers of rare-earth ions separated by tightly bound Si-Rh-Si trilayer blocks that is schematically shown in Fig. 1. Since the chemical bonding between the rare-earth atoms and the adjacent Si-layer is much weaker than within the Si-Rh-Si stacks, the samples can easily be cleaved, leading to structurally well defined Si or Sm-terminated surfaces, respectively [14]. This fact allows for a clear discrimination of bulk and surface derived features in the photoemission experiment. While about 60% of the $4f$ emissions from a RE-terminated surface originate from the rare-earth surface layer, $4f$ emissions from a Si terminated surface stem predominantly from rare-earth atoms situated in the fourth subsurface layer and may be considered to reflect bulk-like properties [15]. Our ARPES experiments on the $YbIr_2Si_2$ system have shown that the information obtained in this way, like the energies of crystal-field split $4f$ states, can be rather useful for the explanation of bulk derived properties like, for example, the specific heat [16].

Performing experiments on $SmRh_2Si_2$, we have first focused on the identification of the surface termination and then on emphasizing the $4f$ signal from Sm atoms by means of resonant photoemission at the $4d \longrightarrow 4f$ excitation threshold. All the experiments were performed for the AFM ordered phase of $SmRh_2Si_2$ single crystals at $T = 10$ K.

$SmRh_2Si_2$ crystallizes in the body-centered tetragonal $ThCr_2Si_2$ (I) type structure ($I4/mmm$ space group, No.139), the so-called 122 phase. It reveals stacks of alternating atomic layers consisting only of one chemical element (–Rh–Si–Sm–Si–Rh–).

The experimentally determined lattice constants are $a = 4.053$ Å and $c = 10.030$ Å (see Ref. [17]). The atomic positions in the unit cell are Sm(0, 0, 0), Rh(0, 0.5, 0.25), and Si(0, 0, 0.37). The body-centered lattice is formed by Sm ions that are eightfold coordinated by Rh atoms at a distance of 3.224 Å. These atomic structure parameters were used for electronic band structure calculations. For the bulk, we have used an enlarged (double-volume) unit cell that contains two formula units and has simple tetragonal symmetry ($P4/mmm$ space group, No.123). This gives us the opportunity to model the characteristic AFM structure of the system, which reveals ferromagnetic order within the Sm planes, while neighboring planes are coupled antiferromagnetically to each other along

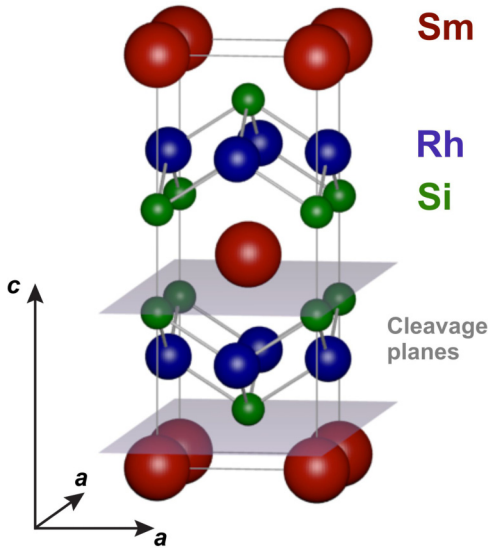

FIG. 1. Tetragonal crystal structure of the $SmRh_2Si_2$. The Sm atomic layers are well separated from each other by the tightly bonded Si-Rh-Si trilayer block. The possible cleavage planes between Si and Sm layers are shown in gray.

the c axis. To take into account the surface sensitivity of the ARPES experiments, slab band-structure calculations have been performed in order to compare the electronic states computed for the bulk with those at the (001) surface of the crystal.

The number of layers used to construct the slab is a compromise between computational time needed and the information about the surface-to-bulk relation, which is intended to be obtained. Increasing the number of atomic layers in the slab maps all dispersions with respect to k_z onto the (k_x, k_y) plane resulting in a two-dimensional representation of the bulk band structure, projected onto the square "surface" Brillouin zone (BZ). In the present work, we have chosen a slab consisting of 24 atomic layers with two differently terminated surfaces (by Si and Sm atoms, respectively). An advantage of such a choice is the preservation of the stoichiometric composition of the system. Note, however, that in this way symmetry operations with $z \longrightarrow -z$ are lost and the symmetry is reduced to the space group No. 99, $P4mm$.

II. COMPUTATIONAL DETAILS

Density-functional theory (DFT) based on the local density approximation (LDA) has successfully been applied to many kinds of materials and has become an efficient tool for first-principle band-structure calculations in solid state physics [18]. However, LDA fails to describe the electronic structure and properties of rare-earth atoms due to the strong correlation interaction between the $4f$ electrons.

A rigorous formulation for the quasiparticle properties in solids is the Green's function approach. The self-energy $\Sigma = G_0^{-1} - G^{-1}$ of the single-particle Green's function G is energy dependent and yields the correlation corrections to the single-particle (mean-field) approximation for the quasiparticle excitation spectrum described by G_0. With a number of plausible assumptions, a LDA+U approach may be applied [19] that results in a correlation correction to the mean-field approximation of the self-energy by means of an additional potential U_{eff}, which shifts the levels of strongly correlated states away from the Fermi level, reducing incorrect hybridization with conduction states, which otherwise spoils the calculated ground-state spin density.

We have adopted this method [20] as a suitable model to treat the on-site $4f$ electron-electron correlations using the rotationally invariant LDA+U approach described in details in Ref. [21]. The on-site Coulomb repulsion U was considered as an adjustable parameter and was chosen equal to 7.0 eV that is in accordance with the experimentally observed [22] $4f$ binding energies (BE). For the exchange integral J, a value of 1.0 eV was assumed from constrained LDA calculations. It should be noted that similar values of these parameters have been used in our previous electronic structure calculations for Sm, Gd, Tm, and Yb compounds [23–26] that provided a very good agreement with experimental data. The calculations of the electronic structure for $SmRh_2Si_2$ were performed using the fully relativistic spin-polarized version [27] of the linear-muffin-tin-orbital (LMTO) method [28]. The Perdew-Wang parametrization [29] for the exchange-correlation potential was used. Brillouin zone integrations were performed by means of the improved tetrahedron method [30].

III. RESULTS OF CALCULATIONS

The LDA+U calculations for the bulk of the $SmRh_2Si_2$ with $U_{\text{eff}} = U - J = 6$ eV yield two independent self-consistent solutions with divalent Sm^{2+} and trivalent Sm^{3+} ions (Fig. 2). Energy analysis shows that both solutions have very close total energies, whereby the Sm^{2+} solution is energetically slightly favorable as compared to the trivalent one. Unfortunately, the LDA+U method, which combines LDA with a basically static, i.e., Hartree-Fock-like mean-field approximation for the multiband Anderson lattice model

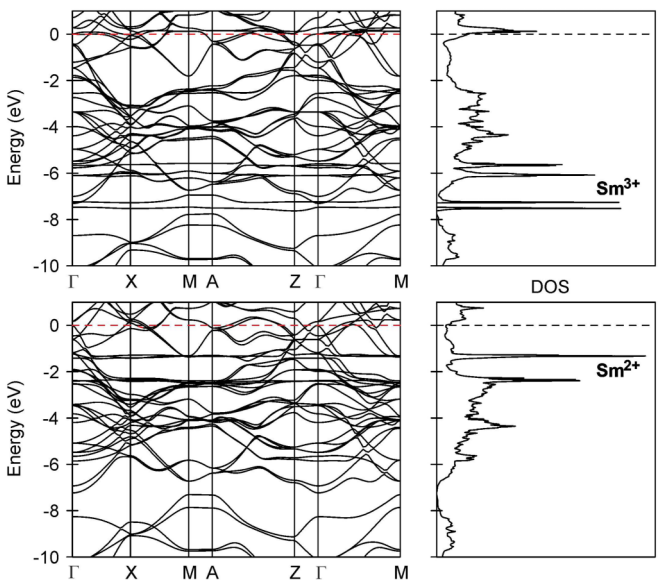

FIG. 2. Calculated energy band structure and total density of states for solutions with trivalent (upper panel) and divalent (lower panel) Sm atoms in the bulk of the $SmRh_2Si_2$.

cannot properly describe the energy band structure at finite temperatures. Thus it cannot be excluded that for nonzero temperatures the trivalent solution becomes more preferable. This question can only be clarified from comparison with the experimental data. Nevertheless, it is important to note that two different but energetically almost degenerate solutions (for Sm^{2+} and Sm^{3+}) can be obtained independently and self-consistently for $U_{\text{eff}} \geqslant 6$ eV. For smaller values of U_{eff} only the Sm^{2+} solution is obtained, which is not consistent with the experiment.

It can be seen in Fig. 2 that flat $4f$-derived bands of Sm^{3+} are located between -5.8 and -7.5 eV whereas the bands of Sm^{2+} can be found between -1.3 and -2.5 eV. It should be noted, that self-consistency of the calculations leads easily to the Sm^{2+} solution in contrast to calculations for Sm^{3+} that should be performed very carefully due to the presence of the unoccupied $4f$ state of the trivalent Sm ion just above the Fermi level and close to conduction band states, which begins to fill even for insignificant changes of the potential and causes instabilities in the process of the self-consistent calculations.

The energy structure of the valence bands is very similar for both (divalent and trivalent) solutions except for the energy regions of the Sm $4f$ states which induce certain noncrossing effects and small energy shifts of the valence bands. The flat bands of Sm $4f$ states appear in the density of states (DOS) as narrow peaks that are split due to spin-orbit coupling as well as the Zeeman effect. Of course, the single-particle approach of LDA+U cannot reproduce the final-state Sm $4f^{n-1}$ multiplet structure observed in photoemission experiments, but our calculations still correctly describe the binding energies of the $4f^{n-1}$ Hund′s rule ground states in the photoemission spectra [compare the features around 6 eV BE in Fig. 3 (theory) and in Fig. 4 (experiment)].

Taking into account the surface sensitivity of the PE measurements we have also performed slab calculations for Si and Sm-terminated surfaces. Assuming a trivalent state of Sm ions in the bulk as it follows from the photoemission experiments presented below, we have fixed the Sm^{3+} solution for the slab layers except for the surface Sm layer where again energetically almost degenerated solutions for trivalent and divalent Sm ions have been found independently. Note that no surface relaxation has been considered although at least in a case of divalent Sm ions an outward relaxation might be expected from the enlarged ionic radius of the divalent with respect to the trivalent configuration. However, as will be shown in Sec. V, Sm ions in an outermost surface layer of $SmRh_2Si_2$ behave almost trivalent as in the bulk making explicit consideration of divalent surfaces unnecessary. The calculated DOS (broadened by a Gaussian with $\sigma = 0.15$ eV) of Sm $4f$ states for different atomic layers in the slab are presented in Fig. 3.

The energy position of the Sm $4f$ bands for the atomic layers buried deep in the slab is very similar to that obtained from the bulk calculations, with only minor changes of the fine structure of the DOS. For the Sm-terminated surface, the position of the Sm^{3+} $4f$ bands reveals an energy shift of $\sim$0.35 eV towards higher binding energies with respect to the bulk corresponding to the surface core-level shift observed in photoemission.

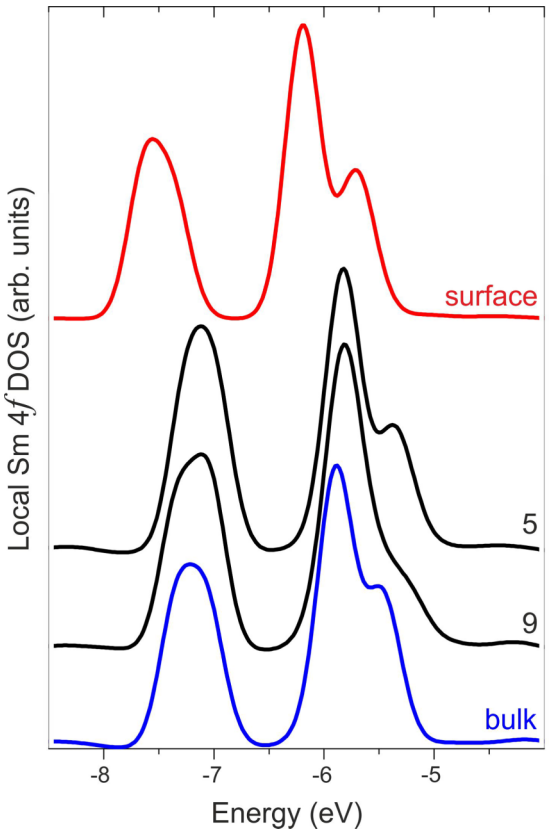

FIG. 3. Calculated local $4f$ densities of states for buried Sm layers in the slab model as compared to those at the Sm-terminated surface and the results of the bulk calculations. The numbers correspond to the Sm layer position with respect to the Sm-terminated surface.

Unfortunately, our calculation method gives no possibility to describe Sm atoms in a homogeneous mixed valence state between the divalent and trivalent configurations. However, taking into account that the obtained divalent and trivalent solutions are almost degenerated energetically, one could expect mixed valence in the $SmRh_2Si_2$ compound.

IV. DETAILS OF THE EXPERIMENT

High-quality single crystals of $SmRh_2Si_2$ were grown by a high-temperature indium-flux method with similar parameters as reported for $GdRh_2Si_2$ [31]. ARPES experiments were performed at the I05 beamline of Diamond Light Source (DLS). Before the measurements the sample was cleaved *in situ* under ultra-high vacuum conditions (10^{-11} mbar range) at a temperature of 10 K. By inspection of the ARPES signal as a function of the beam position on the sample, surface regions were identified that were almost completely terminated either by Si or Sm atoms. Then, resonant ARPES data were taken from respective surfaces at photon energies across the $4d \longrightarrow 4f$ threshold of Sm allowing to enhance the $4f$ emission for divalent and trivalent Sm configurations exploiting the Fano-Beutler resonances [32] of the photoionization cross sections. All measurements were performed at a temperature of 10 K.

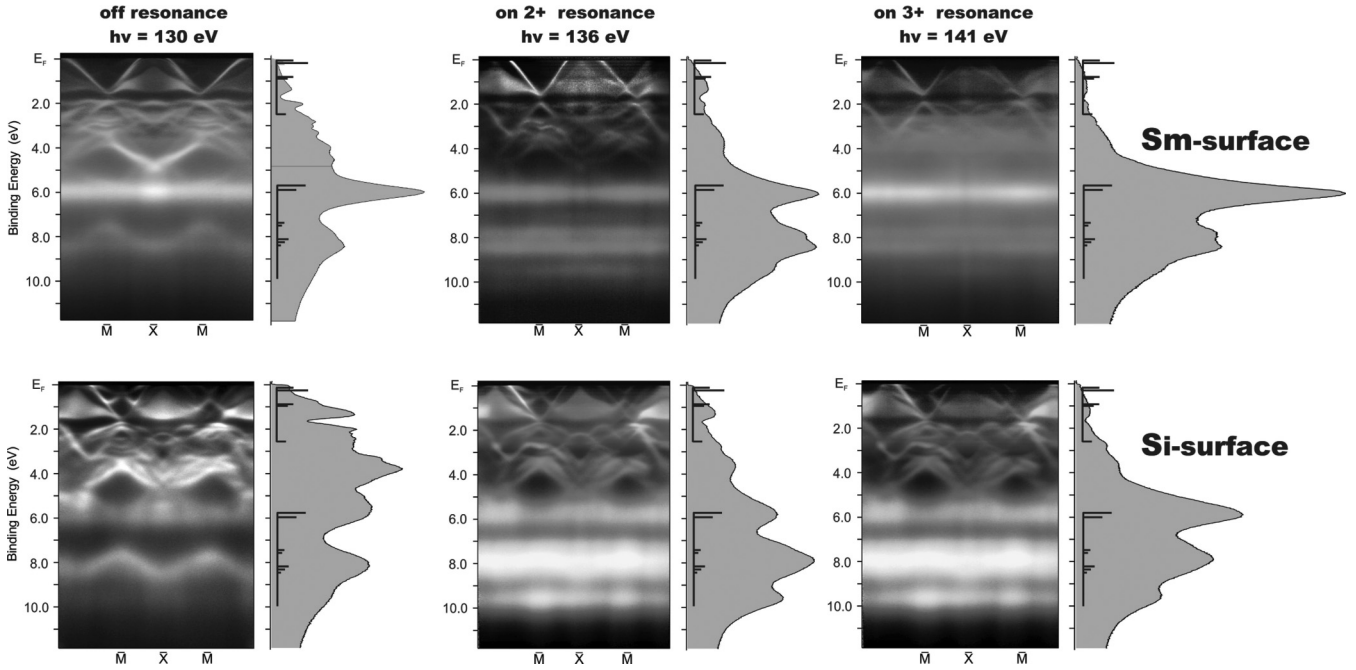

FIG. 4. k-resolved and k-integrated photoemission spectra along the $\overline{\mathrm{X}}$-$\overline{\mathrm{M}}$ direction for Si- and Sm-terminated surfaces at photon energies in off-resonance (130 eV), "on 2+" resonance (136 eV), and "on 3+" resonance (141 eV) regimes.

V. PHOTOEMISSION RESULTS

Our previous angle-resolved PE studies on other members of the same family of RET_2Si_2 compounds (RE = Yb, Eu, Ce, and Gd, while T = Rh, Ir, and Co) demonstrated that their layered structure allows for preparation of atomically clean surface covered by either RE or Si atoms. Si-terminated surfaces are characterized by the presence of an intense Shockley surface state situated in a broad gap of the projected bulk band structure around the $\overline{\mathrm{M}}$ point of the surface Brillouin zone [33–35]. This pronounced feature is absent for Sm-terminated surfaces and can be used to discriminate a Si-terminated surface from a Sm-terminated one.

We begin with a general discussion of the bulk $4f$ spectral function. Variation of the photon energies leads to changes of the photoionization cross sections and allows to distinguish contributions from different atomic states to the PE spectra. In the *on*-resonance spectra, the $4f$ PE intensity is strongly enhanced by the mentioned Fano-Beutler resonance due to constructive interference of the direct $4f$ photoionization channel with an excitation of a core electron into the $4d^9 4f^{n+1}$ intermediate state which decays via super-Coster-Kronig transition into the same $4d^{10}4f^{n-1}$ final state as in direct $4f$ PE. In the *off*-resonance spectra, on the other hand, valence-band emissions (mainly from Rh $4d$ states) dominate due to a destructive interference of the two excitation channels. According to the x-ray absorption spectrum, the Sm^{2+} component is enhanced at 136 eV photon energy (at the $4d \rightarrow 4f^6$ x-ray absorption edge), whereas the Sm^{3+} component is enhanced at 141 eV (at the $4d \rightarrow 4f^5$ absorption threshold). In order to simplify the description, we will use the notations "on 2+" and "on 3+" resonances, respectively. In order to study valence-band contributions, the *off*-resonance spectra at 130-eV photon energy were used.

Figure 4 shows a series of valence-band PE spectra ranging from off to on resonance taken from Si- and Sm-terminated surfaces of $SmRh_2Si_2$. Presented angle-integrated spectra were obtained by k integration along the $\overline{\mathrm{M}}$-$\overline{\mathrm{X}}$-$\overline{\mathrm{M}}$ direction in k space and normalized in intensity to the background at 10–12-eV BE. The off-resonance spectra reveal for both surface terminations between the Fermi energy and 5-eV binding energy intense contributions from the valence-bands which are superimposed by residual Sm $4f$ emissions at higher BE. At increasing photon energies the valence-band contributions are strongly reduced and in the on-resonance region the shape of the PE spectra is determined by Sm $4f$ states. In agreement with the results of our band-structure calculations, the broad $4f^4$ final-state multiplet of trivalent Sm is observed between 6- and 10-eV BE, whereas $4f$ emissions from divalent Sm are expected near the Fermi energy.

The transition from the $4f^5$ ground state $^6H_{5/2}$ of trivalent Sm to the $4f^4$ final states yields a characteristic three-peaked structure in the PE spectrum divided into: (i) a group of ^{5}I states at ∼6-eV BE, (ii) a group of ^{5}F and ^{5}G states at 8-eV BE (apparently, not resolved in PES), and (iii) a group of ^{5}D states reflected only by a shoulder at ∼9.5-eV BE. The observed multiplet structure may be described by results of free-atom calculations in intermediate coupling scheme [36]. However, it should be noted, that the resonant excitation may lead to intensity deviations of certain multiplet terms from the results of free-atom calculations performed for nonresonant $4f^n \rightarrow 4f^{n-1}$ dipole excitations. This is mainly due to the complex multiplet structure of the $4d^9 4f^{n+1}$ intermediate state which leads to an resonant enhancement of certain multiplet terms at different photon energies (see Fig. 4).

Possible divalent Sm $4f$ contributions to the PE spectrum are expected close to the Fermi level. According to the free-atom calculations for $4f^6 \rightarrow 4f^5$ transitions [36], the

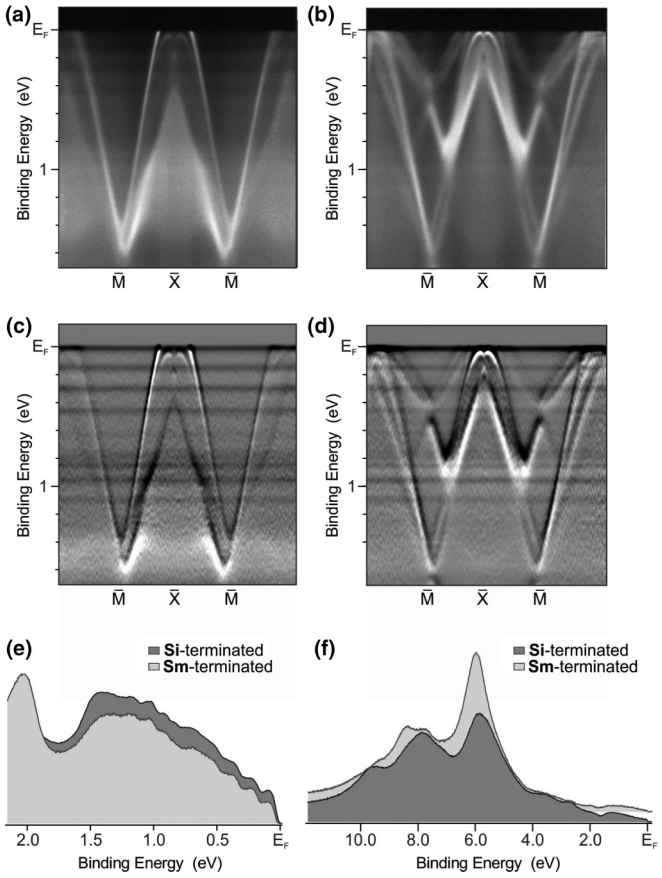

FIG. 5. ARPES data near the Fermi level taken from the Sm- [(a) and (c)] and Si-terminated [(b) and (d)] surface at 136-eV ("on 2+" resonance) photon energy presented as measured [(a) and (b)] and with improved contrast by means of the first derivative [(c) and (d)]. Respective angle-integrated spectra are shown for both surface terminations in (e). (f) Angle-integrated spectra taken at 141-eV photon energy ("on 3+" resonance) for both surfaces.

respective final-state multiplet consists of (i) a group of ^{6}H states at lowest BE (according to the Hund rule, the state $^6H_{5/2}$ is the ground state for the $4f^5$ configuration), (ii) a group of ^{6}F states shifted by about 1 eV to higher BE, and (iii) a group of ^{6}P states with much weaker intensities expected between 2.9- and 3.5-eV BE. Respective emissions have been observed experimentally for Sm metal [37] as well as for several Sm compounds like $SmAl_2$ (Ref. [38]), SmS (Refs. [39,40]), SmB_6 (Ref. [3]), and $SmSn_3$ (Ref. [12]). For the trivalent systems, emissions from divalent Sm could mostly be identified as results of surface valence transitions. In case of $SmSn_3$, also divalent bulk signals were reported [12], which were assigned to weak divalent $4f^6$ admixtures to the trivalent $4f^5$ ground state.

In contrast to the mentioned systems where the $4f^5$ final-state contributions represent a significant part of the total $4f$ spectral intensities, we observe independent from the actual surface termination only relatively weak divalent components for $SmRh_2Si_2$. Figures 5(a) to 5(d) show ARPES data taken at the Sm "on 2+" resonance for both of Sm- and Si-terminated surfaces, respectively, which reveal fine, largely nondispersive stripes, which also extend over the region of the gaps of the projected band structure around the $\overline{M}$ points of the surface Brillouin zones and, therefore, clearly represent spatially strongly localized final states. From the fact that these structures become enhanced "on 2+" resonance, they may be attributed to the $4f^5$ final-state multiplet of divalent Sm. Figure 5(e) shows the respective angle-integrated data for both surface terminations, which reveal clearly a multiplet structure consisting of two sets of lines, one situated close to the Fermi energy (^{6}H final-state configuration) and the other starting at about 0.9-eV BE (^{6}F final-state configuration). Assuming a mean free path of 5 Å for photoelectrons with a mean kinetic energy of about 135 eV, then the $4f$ signal from the outermost atomic surface layer of a Sm-terminated $SmRh_2Si_2$ sample amounts to about 60% of the total $4f$ emission, while in case of a Si-terminated surface the $4f$ signal corresponds to a pure bulk emission. However, as can be seen in Figs. 5(e) and 5(f), the relative emission intensities from divalent Sm with respect to the total $4f$ emission differ only slightly for Si and Sm terminated samples.

From the fact, that shape, energy position and intensity of the $4f^5$ multiplets are almost the same for both surface terminations we may conclude that the electronic properties of bulk and surface are rather similar and the Sm ions behave in both cases slightly mixed-valent. A mixed-valent character of Sm in the bulk and at the surface is additionally supported by the observation, that the $4f^5$ multiplet is in both cases obviously pinned to the Fermi energy indicating energy degeneracy with the ground state. Since the relative intensity of the $4f^5$ component is very small as compared to the trivalent $4f^4$ signal (see *on*-resonance spectra shown in Fig. 4), the Sm valence in the compound is obviously close to trivalent with weak divalent admixtures to the ground state. Since the weak Sm^{2+} signals are superimposed by a background of valence-band emissions (which vary their intensities with photon energy) and $4f^4$ and $4f^5$ final-state components resonate at different photon energies, it is difficult to evaluate the Sm valence. Nevertheless, from the relative intensities of the divalent and trivalent components the mean valence of the Sm ions in $SmRh_2Si_2$ may roughly be estimated to be not smaller than 2.9. More precise results might be obtained from core-level spectroscopies, a high-precision determination of the mean valence is, however, beyond the scope of the present work. We could yet not detect a reliable signature of this slightly mixed valent state in bulk properties, e.g., in magnetic ones. This might be due to two effects. On the one hand, RKKY exchange interactions are pretty large in $SmRh_2Si_2$, and could thus easily mask the weaker effects of hybridization. On the other hand, the $4f^6$ configuration of Sm^{2+} has a very large Van Fleck susceptibility, which is one order of magnitude larger than that of Pauli paramagneticic Ce^{4+} or Yb^{2+} systems. Thus in this sense Sm^{2+} is much more magnetic than Ce^{4+} and Yb^{2+}, and therefore differences in magnetic properties to a pure trivalent Sm state might be more difficult to detect.

A mean valence close to Sm^{3+} is also supported by the known AFM order of Sm $4f$ moments in the bulk. Observation of a magnetic exchange-splitting of the surface state at the $\overline{M}$ point [Figs. 5(b) and 5(d)] implies ferromagnetic order of Sm $4f$ states in the fourth atomic layer below the Si-terminated surface. Similar splittings have been observed and discussed in details [33,35] for $EuRh_2Si_2$ and $GdRh_2Si_2$.

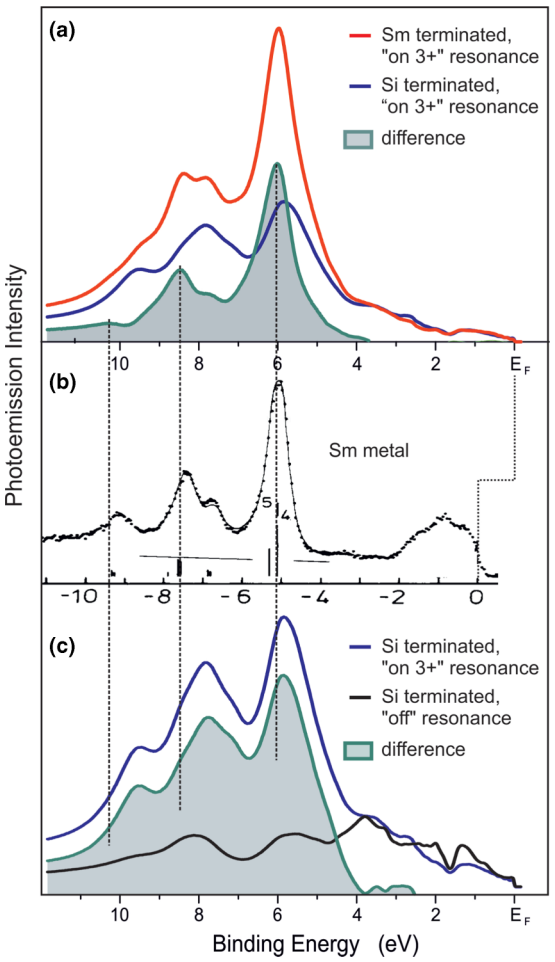

FIG. 6. Difference of PE spectra taken from Sm- and Si-terminated surfaces "on 3+" resonance (surface contribution of the trivalent Sm – grey area) (a), PE spectrum of trivalent Sm metal taken with Mg $K\alpha$ radiation at 1253.6 eV photon energy [22] (b), and difference of PE spectra taken from Si-terminated surface taken "on 3+" resonance and off-resonance (bulk contribution of the trivalent Sm: grey area) (c).

The fact that the Sm ions at the surface behave trivalent or slightly mixed-valent can also be concluded from a closer inspection of the $4f^4$ multiplet spectra shown in Fig. 5(f), which reveals clear differences in the spectral shape depending on the surface termination. The well defined surface termination allows to extract $4f$ bulk and surface components from a subtraction of spectra taken from differently terminated surfaces or taken at different resonance conditions, respectively. Figure 6(a) shows the difference of PE spectra taken from Sm- and Si-terminated surfaces at 141 eV photon energy ("on 3+" resonance). The spectra are normalized to equal intensities in the region 3.5–4.0 eV BE where no $4f$ emissions are expected and the spectra are dominated by valence-band emissions (both Rh $4d$- and Si $3s3p$-derived states), which are eliminated in the difference spectrum. The latter reflects the trivalent Sm $4f$ surface emission and reveals the well-known Sm^{3+} multiplet structure. As compared to a reference spectrum of trivalent Sm metal taken at 1253.6 eV [22] [see Fig. 6(b)], the spectrum reveals a rigid energy shift of 1.0 eV towards higher BE as well as a strongly reduced intensity of the ^{5}D term caused by the different enhancement of individual multiplet components across the $4d \rightarrow 4f$ excitation threshold. The energy shift reflects the effects of both the altered chemical environment in the compound with respect to the pure metal and the reduced atomic coordination at the surface. Apart from this energy shift and the mentioned minor intensity variation the spectrum looks very similar to that of the pure metal.

In order to extract the shape of the $4f$ bulk emission, the difference between an on-resonance and an off-resonance spectrum from identical Si-terminated surfaces taken at 141- and 130-eV photon energy, respectively, was considered again normalized at around 4.0-eV BE. Figure 6(c) shows the result of this subtraction. Unfortunately, extracting the shape of the $4f^4$ final-state bulk multiplet by exploiting the resonant $4f$ cross-section variations across the excitation threshold is less precise because the shape of the underlying valence bands may also be altered as a function of photon energy [41]. Stronger cross-section variations might be expected for Rh $4d$ derived states which reveal a Cooper minimum below 120-eV photon energy leading to smoothly increasing cross-sections between 130 and 140 eV, while Si $3s3p$ cross-sections decrease in the same photon-energy range by about 10%. However, since the intensity of the valence-band background does not exceed 30% of the $4f$ emission intensity, the effect of these cross-section variations may be neglected. As compared to the $4f^4$ surface emission the bulk-derived difference spectrum is strongly broadened. Spectral broadening by energy splittings of individual multiplet components may qualitatively be explained by hybridization between $4f$ and valence-band states and have been observed across the whole *RE* series [42–44].

A closer inspection of the difference spectra shows that the surface component reveals a systematic shift of the order of 0.2–0.7 eV towards higher BE with respect to the bulk emission. The value of this surface core-level shift (SCS) is in fair agreement with the results of the slab band-structure calculations for the Sm-terminated surface (Fig. 3). A SCS of the trivalent Sm $4f^4$ multiplet has to our knowledge never before been reported since most trivalent Sm systems undergo a surface valence transition to the divalent state and trivalent surface emissions are consequently not present. The size of the observed surface energy shift for Sm^{3+} looks comparable to the SCS exceeding 0.7 eV observed [45,46] for the divalent $4f$ emissions in the isostructural compounds $EuRh_2Si_2$ and $YbRh_2Si_2$. It should be also noted, that assuming a mixed-valent Sm character in the $SmRh_2Si_2$ compound, we could not expect a SCS for the $4f^5$ multiplets because the final-state component with larger $4f$ occupancy is always pinned to the Fermi energy since the lowest lying term of the final-state multiplet is energetically degenerate with the ground state.

In the paper of H. Yamaoka *et al.* [12] on $SmSn_3$, a spread of the ^6H_J states of the $4f^5$ multiplet across the Fermi energy was stated on the basis of LDA+DMFT calculations where the Sm $4f$ states were treated with the Hubbard I approximation. To our opinion, this is an artifact of the calculation caused by the mixed-valent character of the system. As it was mentioned above, the final-state multiplet line with the smallest binding energy reproduces the trivalent $^6H_{5/2}$ ground state of the system and is, therefore, pinned to the Fermi level. The other five ^6H_J terms are excited final states

and are observed in photoemission at higher BE with energy spacings of about 0.12 eV. We attribute, therefore, the whole spectral region between Fermi energy and 0.7-eV BE to the ^6H_J terms from which five lines are clearly resolved (see Fig. 5). The free-atom calculations [36] performed for $4f^6 \rightarrow 4f^5$ transition provide significant intensities only for the two leading terms ($^6H_{5/2}$, $^6H_{7/2}$) whereas intensities of the other components are predicted to be smaller than 1%. In the experiment, however, the $4f^5$ final state does not arise from the Hund rule $4f^6$ ground state of stable divalent Sm as assumed for the calculation but from weak $4f^6$ admixtures to a trivalent $4f^5$ ground state excited under resonant conditions. The intensities of the individual terms of the multiplet may, therefore, strongly deviate from the results of the free-atom calculations. The total width of 0.7 eV and the line splittings of the ^6H multiplet calculated by H. Yamaoka *et al.* [12] are in agreement with our results, however the whole multiplet is shifted upwards in energy so that four terms are lying above the Fermi energy. Due to this shift of the ^6H multiplet the spectral region between 0.5 and 0.7 eV BE was attributed to emissions from divalent Sm surface atoms shifted in energy by a SCS of 0.5 eV. On the background of the similarity of the spectra obtained from Si- and Sm-terminated surfaces such an interpretation of the PE spectra seems to be rather unlikely for the present case.

In the free-atom multiplet calculations, the sextet ^6H_J term is followed by the sextet ^6F_J term shifted with respect to the former by 0.9 eV for which again only the two most intense lines are listed [36]. The LDA+DMFT calculations [12] locate these terms at ∼0.9-eV BE and predict a spread of the line splittings of about 0.3 eV. Our measurements resolve in fact peaks at about 0.85, 0.95, and 1.1 eV BE (see Fig. 5) followed by a broader peak at about 1.4 eV and a deep minimum at 1.75-eV BE. The feature at 1.4 eV and a further peak at 2-eV BE might be related to underlying valence-band emissions since the next term of the $4f^5$ final-state multiplet (^6P) is only expected at 2.8-eV BE.

VI. DISCUSSION

As free atoms, all *RE* elements except La, Gd, and Lu reveal a divalent $[Xe]4f^n6s^2$ ground-state configuration, while with the exception of Eu and Yb they behave trivalent in the condensed phase. The reason for this valence transition is that the energy $U_{f\rightarrow d}$ needed to excite a $4f$ electron into an unoccupied $5d$ orbital, i.e., to transform the atom from the divalent into the trivalent state, may be compensated in solids by the gain in cohesive energy in the trivalent state, $\Delta E_{\rm coh} = E^{3+}_{\rm coh} - E^{2+}_{\rm coh} > 0$. In order to determine the valence of *RE* ions in solids and the related $4f$ binding energies B. Johansson proposed [47] a simple thermochemical approach: based on measured $4f$ excitation energies of *RE* elements in the gas phase and the excess in cohesive energy between typical trivalent and divalent metals Johansson constructed a diagram that visualizes the excitation energy $\Delta E_{\rm II,III} = U_{f\rightarrow d} - \Delta E_{\rm coh}$ needed to transform the ions in the pure metals from the divalent to the trivalent state (see Fig. 7, left panel).

The respective energy zeros for free atoms as well as bulk and surface of pure metals are visualized by horizontal lines that divide the diagram into trivalent regions above and divalent

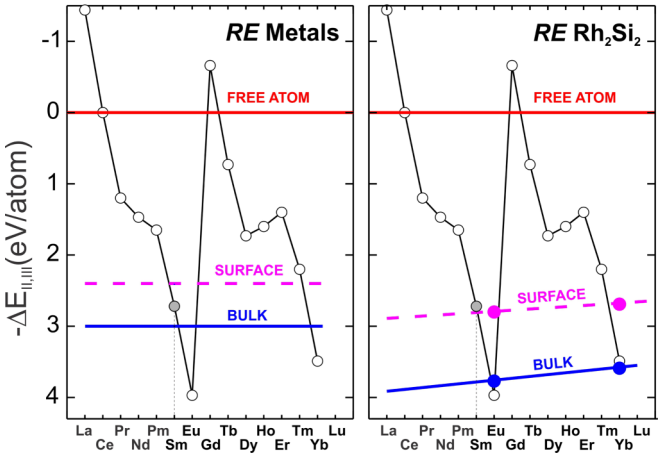

FIG. 7. The excitation energy $\Delta E_{\rm II,III}$ necessary to transform the divalent into a trivalent configuration for *RE* metals (left) and *RE*Rh_2Si_2 compounds (right). The red line defines the zero of energy for the free atoms, open circles mark the values of $U_{f\rightarrow d}$ for individual *RE* elements in the gas phase. The blue solid and magenta dashed lines indicate the position of the energy zeros in the bulk and at the surface after consideration of the respective gains in cohesive energy.

regions below the lines, respectively. For *RE* metals, $\Delta E_{\rm coh}$ equals 3 eV and shifts the reference zero from the red line ("FREE ATOM") down to the blue line denoted as "BULK". As is evident from the energy position of the latter, only Eu and Yb reveal positive $\Delta E_{\rm II,III}$ values corresponding to stable divalent ground states in the bulk whereas all other *RE* metals lie in the trivalent region above this line. At closed packed surfaces, cohesive energies are reduced to about 80% of their bulk values and as a consequence the respective reference zero for the surface is shifted with respect to the bulk by about 0.6 eV upwards arriving at the position marked by the dashed line denoted as "SURFACE". Sm metal reveals a $\Delta E_{\rm II,III}$ value below the respective surface reference zero indicating the stabilization of a divalent Sm layer at the surface of a trivalent bulk. This surface valence transition of Sm was in fact observed experimentally [3,37].

In *RE*-based materials, the cohesive energies of the pure metals are altered by the formation enthalpies leading to shifts and tiltings of the reference-zero lines. In order to create a similar diagram for *RE*Rh_2Si_2 compounds, we could make use of measured binding energies: assuming full screening of the final state, photoemission describes also the excitation of a divalent $[Xe]4f^n6s^2$ to a trivalent $[Xe]4f^{n-1}(5d6s)^3$ state. In contrast to the calculation of $\Delta E_{\rm coh}$, however, which considers the difference in cohesive energies between homogeneous trivalent and divalent systems, PE describes a $4f$ excitation of a single ion embedded in the matrix of the divalent solid. As a consequence, the measured BE differs from $\Delta E_{\rm II,III}$ by the so-called impurity term $E_{\rm imp}$, which describes basically the solution enthalpy of a trivalent ion in a divalent metal at the limit of infinite dilution. The magnitude of this quantity depends on the atomic volumes, electronegativities, and electron densities in the divalent and trivalent state and may be estimated within the semi-empirical Miedema scheme [48] to 0.6 eV for pure *RE* metals [38]. In fact, the BEs for divalent Eu and Yb metal, 1.6 and 1.1 eV, calculated as $\Delta E_{\rm II,III} + E_{\rm imp}$

are close to the measured BEs of 1.8 and 1.2 eV, respectively. In compounds, however, E_{imp} can usually be neglected since di- and trivalent *RE* systems of the same compound series differ only weakly in their lattice constants and are, therefore, usually arbitrarily miscible indicating that the solution enthalpies are close to zero or even slightly negative. This fact may be used to construct respective $\Delta E_{\mathrm{II,III}}$ diagrams for the whole series of isostructural *RE* compounds by determining the reference zeros for bulk and surface from measured $4f$ BE energies of a single divalent compound [38].

Applying this approach to the $RE\mathrm{Rh_2Si_2}$ compound series we may use PE data of the divalent compound $\mathrm{EuRh_2Si_2}$, where the BEs of the $4f^6$ final state are equal to 0.2 eV in the bulk and 1.1 eV at the surface [45]. Additionally, using PE results from the compound $\mathrm{YbRh_2Si_2}$, which is mixed-valent in the bulk but divalent at the surface, we find a BE of the $4f^{13}$ final state in the Yb surface layer of 0.8 eV [46,49]. An analysis of the mixed-valent Yb bulk state by means of the Single-Impurity Anderson Model (SIAM) localizes the unhybridized $4f^{14}$ component at about 0.1 eV above the Fermi energy [46]. Based on these data, we may construct the diagram for the whole $RE\mathrm{Rh_2Si_2}$ series of compounds (Fig. 7, right panel). Here, filled circles reveal the Fermi level positions with respect to the measured binding energies of divalent bulk and surface components in the PE spectra of $\mathrm{EuRh_2Si_2}$ and $\mathrm{YbRh_2Si_2}$, respectively. The positions of the energy zeros for bulk and surface (blue full and magenta dashed lines) are obtained by linear interpolation between the respective Fermi level positions of these two compounds. It should be noted, that assuming surface cohesive energies reduced to 75% of their bulk value we get the respective surface reference line that coincides exactly with that obtained from the PE data. This confirms the consistency of the photoemission and thermochemical approaches. The reference-zero lines do not run horizontally as sketched for the pure metals but are slightly inclined reflecting systematic variations in the heat of compound formation caused by the different size of the ions in the course of lanthanide contraction.

Considering now the $\mathrm{SmRh_2Si_2}$ compound, we arrive at the prediction that Sm is located above both "BULK" and "SURFACE" lines, indicating that the Sm ions behave trivalent both in the bulk and at the surface. Classical valence fluctuations in the sense of the Falikov-Kimball model [50] can be excluded since they demand energy degeneracy of adjacent $4f$ configurations within an energy scale of $k_BT \approx 30$ meV. A valence-fluctuating state, where intermediate valence is caused by thermal transitions between energetically almost degenerated states, corresponds in Fig. 7 to a scenario, where the "BULK" (or "SURFACE") line goes just through an open circle.

Larger energy difference, however, may be bridged by hybridization between the $4f$ states and valence states, which results in quantum mechanical mixing of different f states and thus to a mixed valent ground state. This mechanism and the related phenomena have been extensively studied in Ce systems. Because the divalent $\mathrm{Ce^{2+}}$ with $4f^2$ and the tetravalent $\mathrm{Ce^{4+}}$ with $4f^0$ configuration are located at about 4 eV and 2 eV above the Fermi level, respectively [44], one would expect these Ce systems to be in a stable trivalent $\mathrm{Ce^{3+}}$ with $4f^1$ configuration.

Nevertheless, many Ce compounds behave homogeneous mixed-valent with a mean valence around 3.1–3.2 as concluded from the PE spectra that reveal a well-known double-peaked $4f$ emission consisting of a "$4f^0$ ionization peak" at about 2-eV BE and a "$4f^1$ hybridization peak" just at Fermi level, which is usually related to the Kondo-resonance. The $4f$ configurations in a strongly hybridized system may be described by linear combinations of eigenfunctions for adjacent atomic $4f^n$ configurations. In case of Ce systems, admixtures of a $4f^0$ configuration to the trivalent $4f^1$ state lead to a mean $4f$ ground-state occupation of about 0.9–0.8. In the photoemission process an atomic-like $4f^0$ state is theoretically produced by emission of a $4f$ electron, but in the solid there exist only mixed eigen-states that leads to the observed double-peaked structure in the experiment. Respective hybridization effects are not restricted to Ce systems but have also been found in Pr and Nd compounds [42] as well as for the heavy rare earths Tb, Dy [43], and particularly Yb compounds, which represent an analog to respective Ce sytems in the light of the electron-hole symmetry [46]. We propose the same mechanism to be responsible for the mixed valent state we observed in the bulk and at the surface of Sm. In the following, we support this proposition by an analysis based on standard approaches used for Ce and Yb systems.

Such hybridization induced mixed phenomena may be described by means of the SIAM. A simple variational solution for the Anderson Hamiltonian may be obtained by a numerical procedure [44] that represents a minimal version of the more elaborated Gunnarsson-Schönhammer approach to SIAM [51]. The mixed-valent states are constructed from the basis $4f^{n-1}$, $4f^n$, and $4f^{n+1}$ configurations at energies 0, ϵ_f and $2\epsilon_f + U_{ff}$, whereby the parameter ϵ_f denotes the energy of a nonhybridized $4f^n$ state and U_{ff} denotes the on-site Coulomb repulsion of two $4f$ electrons at the same atomic site. Allowing for electron hopping between the localized $4f$ states and the valence band, an off-diagonal hybridization matrix element Δ is introduced. Then, diagonalizing the model Hamiltonian yields hybrid states of the form

$$|s\rangle = \sum_k c_k |4f^{(k)}\rangle, \tag{1}$$

where the state with minimal energy corresponds to the ground state $|g\rangle$. The value of Δ that describes the strength of the hopping interaction between the $4f$ and itinerant electron states depends on the localization of the $4f$ wave functions, the interatomic distances as well as on the angular momentum character of the valence states. For a given series of isostructural *RE* compounds, Δ is expected to decrease monotonically from Ce to Yb reflecting increasing localization of the $4f$ shell [42].

Simulations of PE spectra by means of SIAM [52] lead for the Kondo-system $\mathrm{CeRh_2Si_2}$ (Ref. [15]) with the model parameters $\epsilon_f = -1.7$ eV and $\Delta = 1.05$ eV to a Ce valence equal to 3.03, whereas for the heavy-fermion system $\mathrm{YbRh_2Si_2}$ the parameters $\epsilon_f = -0.1$ eV and $\Delta = 0.12$ eV lead to a proper description of the PE spectra resulting in a mean Yb valence of 2.93 [46]. Assuming in a first approximation a linear decrease of the Δ parameter as a function of atomic number a mixed-valent behavior of the Sm ions in $\mathrm{SmRh_2Si_2}$ is rather probable.

TABLE I. SIAM parameters, the contributions of different configurations to the ground state and calculated Sm valence in the bulk and at the surface of the $SmRh_2Si_2$ compound.

SIAM parameters (eV)	Bulk	Surface
ϵ_f	−6.0	−6.3
Δ	0.7	0.5
U_{ff}	7.0	7.0
$c^2(4f^4)$	0.0002	0.0001
$c^2(4f^5)$	0.9363	0.9490
$c^2(4f^6)$	0.0635	0.0509
Sm valence	2.937	2.949

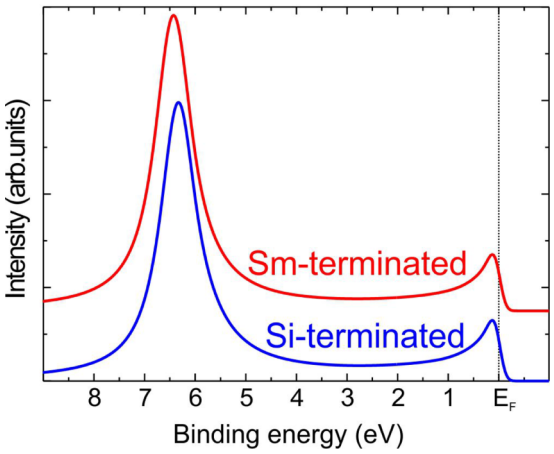

FIG. 8. Calculated model PE spectra of the $SmRh_2Si_2$ compound for the Si-terminated and Sm-terminated surfaces. For the Sm-terminated surface, the contribution from the uppermost Sm layer is taken to be 60% of the total PE intensity.

Unfortunately, in contrast to Ce (or Yb), where starting from an unfilled (or fully filled) $4f$ shell, the behavior of the $4f^1$ (or $4f^{13}$ hole state) configuration is considered in interaction with the adjacent configurations, the model is not directly applicable to the case of the Sm compound due to the presence of several $4f$ electrons in the ground state. Considering $4f^4$, $4f^5$ and $4f^6$ configurations in the basis, we might assume that four electrons behave strictly localized and do not undergo excitation or hybridization effects. In reality, of course, each of the five $4f$ electrons in the Sm $4f^5$ ground state may be subject to hopping processes, and this is one of the reasons why in the PE spectra the whole $4f^5$ multiplet becomes visible. The probability, however, that two $4f$ electrons become excited simultaneously is small, because the energies to produce respective $4f^3$ (or $4f^7$) configurations are large due to the large on-site repulsion energy U. Therefore we only consider excited states that do not contain less than four electrons. Neglecting excitations within the individual $4f^n$ multiplets the hybridization conditions are the same for all $4f$ electrons.

With this assumption we may evaluate hybridization effects by means of the SIAM. Simple linear interpolation between the Δ values of the Ce and Yb compounds leads to an estimate of $\Delta = 0.7$ eV. The value of ϵ_f was chosen to be equal to -6 eV in agreement with the position of the energetically lowest lying ^{5}I multiplet component of Sm^{3+} as observed in the PE spectra. The parameter $U_{ff} = 7$ eV was taken from the LDA + U calculations. For the surface Sm layer a surface core-level shift of 0.3 eV was introduced in accordance with Fig. 6 and the results of our LDA + U calculations, and Δ was reduced to about 70% of its bulk value taking into account a lowering of the hopping probability with decreasing atomic coordination (see, e.g., Ref. [43]). The SIAM parameters and the calculated results are presented in Table I.

Considering the energies of the bare configurations $E(4f^5) = \epsilon_f$ and $E(4f^6) = 2\epsilon_f + U_{ff}$, we obtain for the bulk the energy of the divalent configuration 1 eV above the trivalent one. At the surface this energy difference is reduced to 0.7 eV. If the hybridization is switched on, the ground state becomes mixed-valent with a noticeable contribution of the divalent configuration (about 5%–6%). The calculated mean Sm valence in the bulk amounts to about 2.94, and the difference between the mean valence of bulk and surface Sm ions is very small in accordance with the experiment.

The calculated model PE spectra of the $SmRh_2Si_2$ compound are shown in Fig. 8. The $4f$ multiplet structures are not taken into account in this simplified simulation. Nevertheless, the main features observed in the PE spectra are reflected in the calculated results: there are strong $4f$ emissions at 6 eV and higher BE (related to the trivalent Sm contributions) and an additional peak near the Fermi energy (related to the divalent Sm contribution). The latter is pinned to the Fermi level as was discussed in the preceding section. Its intensity is very close for the Si- and Sm-terminated surfaces indicating an almost identical mixed-valent state of Sm ions in the bulk and at the surface of the crystal, also in agreement with experimental PE data. It is interesting to note that in difference to the $4f$ final-state multiplet lines of the isostructural $EuRh_2Si_2$ [45] and $YbRh_2Si_2$ [34] compounds the individual terms of the Sm $4f^5$ seem not to reveal hybridization gaps or dispersive phenomena around valence-band crossings [compare Figs. 5(a)–5(d)]. This phenomenon might be related to the weakness of hybridization or to different symmetry properties of the $4f^5$ multiplets. It should, however, be borne in mind that the observed $4f$ emissions are only very weak, so that corresponding phenomena may simply not be well seen and distinguished.

In that context, the stable divalent state observed for $EuRh_2Si_2$ remains a puzzle. There, $4f^6$ and $4f^7$ bulk configurations are separated by only 0.2 eV, and extrapolating the large hybridization strength observed in the Sm system one could expect strongly mixed-valent behavior in the Eu compound. Indeed, similar SIAM calculations applied to $EuRh_2Si_2$ (even with reduced hybridization $\Delta = 0.4$ eV) lead to a strong mixing with a mean valence of 2.42. However, it is experimentally well-established that the effect of hybridization is much weaker in Eu based systems than in Ce or Yb based ones [53]. While Ce or Yb systems show in most cases a continuous and weak evolution of the valence as a function of tuning parameter, e.g., chemical composition, pressure, or temperature, Eu systems generally display a very pronounced first order valence transition as a function of the same tuning parameters. In Eu systems, the valence may change directly

from an almost pure trivalent to an almost pure divalent state at these first order transitions, while in mixed valent Ce and Yb systems the valence typically changes by only about 0.1 between 4 and 300 K. The weak and continuous change of the valence in Ce and Yb systems reflects quantum mixing of the different valence states, and therefore the dominant effect of the hybridization. Accordingly these systems are well-described using the Anderson model and related ones. The large changes of valence in Eu systems indicate a dominant on-site $U_{f\to d}$ interaction (which is different from the $U_{f\to d}$ in the Johannson model), and therefore the Falikov-Kimball model is a better approach for describing them [50].

For divalent Eu compounds the $4f$ shell is half-filled and according to Hund's rules all seven $4f$ spins are aligned parallel to each other. Treating hybridization in terms of a hopping mechanism one may restrict oneself to consider, like in case of Sm, only electron hopping between divalent and trivalent configurations since population of a $4f^8$ state is related to an excitation energy of 8 eV [22]. In Sm hopping transitions from the trivalent Hund rule $4f^5$ ground state to a divalent $4f^6$ configurations may be realized either directly or via excitation of virtual low-lying $4f^5$ states of the ^{6}H multiplet term. In case of the divalent Eu $4f^7$ configuration, however, respective transitions to a $4f^6$ state via virtual excitations of low-lying states are blocked. The reason is that all $4f$ states with a given spin orientation are occupied and spin-flip excitations are related to excitation energies of at least 4 eV, as can be seen by inspection of the $4f^7$ multiplet [36]. Respective spin-flip transitions are, on the other hand, more likely in case of Sm^{3+} where the necessary excitation energies amount only to 2.7 eV. Thus, as compared to Sm^{3+}, the number of possible hopping channels is for Eu^{2+} strongly reduced due to the Pauli principle and the half-filling of the $4f$ shell. This leads to a strong decrease of hopping probability, which might strongly suppress hybridization even if the involved excitation energies are small.

VII. SUMMARY

We have presented a theoretical and experimental study of the electronic structure of $SmRh_2Si_2$ focusing on the properties of Sm atoms in the bulk and at the surface. On the basis of the observed $4f^{n-1}$ final-state multiplets ($n = 5$ and 6) in the ARPES data, we found that in both cases the Sm ions behave almost trivalent with weak admixtures of divalent configurations leading to a mean valence of about 2.94 both in the bulk and at the surface. An almost trivalent behavior of Sm ions at the surface could additionally be concluded from the observation of a surface core-level shift of the $4f^{n-1}$ final states. Observation of configurational mixing at the surface of a mixed-valent Sm compound is surprising since even trivalent Sm compounds reveal usually stable divalent surfaces. The Sm ions in $SmRh_2Si_2$ behave in this respect like Ce in most Ce compounds where $4f$ hybridization although reduced survives at the surface.

The observation of a significant divalent admixture in the bulk is also a surprise. Because of fully developed magnetic order and the absence of any evidence of hybridization effects, e.g., in transport properties, Sm in intermetallic compounds is usually considered to be in a very stable and fully trivalent state. The admixture we now observed in $SmRh_2Si_2$ seems to be too weak to significantly affect magnetic order and related properties. Other experiments indicate the formation of a simple AFM structure with ferromagnetic layers coupled antiferromagnetically along the c direction.

This is also supported by our ARPES results: the observation of an exchange splitting of the Shockley surface state at the $\overline{\mathrm{M}}$ point of Si-terminated surfaces, which implies ferromagnetic order of Sm $4f$ moments in the fourth atomic subsurface layer below the outermost Si–Rh–Si trilayer stack. Assuming an almost linear decrease of the hybridization parameter with increasing *RE* atomic number between the isostructural heavy fermion systems $CeRh_2Si_2$ and $YbRh_2Si_2$ (which reflects the effects of lanthanide contraction), the observed divalent admixtures to mostly trivalent Sm ions in $SmRh_2Si_2$ could readily be described by means of the SIAM.

ACKNOWLEDGMENTS

This work was supported by the German Research Foundation (DFG) (Grants No. VY64/1-3, No. GE602/2-1, No. KR 3831/4-1, No. GRK1621, and No. SFB1143), by Research Grant No. 15.61.202.2015 of Saint Petersburg State University as well as by Science and Technology Center in Ukraine STCU, Project No. 6255. We acknowledge Diamond Light Source for experiment on the beamline I05 under proposal SI14811-1.

[1] A. Menth, E. Buehler, and T. H. Geballe, Phys. Rev. Lett. **22**, 295 (1969).
[2] J. W. Allen, B. Batlogg, and P. Wachter, Phys. Rev. B **20**, 4807 (1979).
[3] J. W. Allen, L. I. Johansson, I. Lindau, and S. B. Hagstrom, Phys. Rev. B **21**, 1335 (1980).
[4] M. Dzero, K. Sun, V. Galitski, and P. Coleman, Phys. Rev. Lett. **104**, 106408 (2010).
[5] T. Takimoto, J. Phys. Soc. Jpn. **80**, 123710 (2011).
[6] F. Lu, J.-Z. Zhao, H. Weng, Z. Fang, and X. Dai, Phys. Rev. Lett. **110**, 096401 (2013).
[7] M. Neupane, N. Alidoust, S.-Y. Xu, T. Kondo, Y. Ishida, D. J. Kim, C. Liu, I. Belopolski, Y. J. Jo, T.-R. Chang, H.-T. Jeng, T. Durakiewicz, L. Balicas, H. Lin, A. Bansil, S. Shin, Z. Fisk, and M. Z. Hasan, Nat. Commun. **4**, 2991 (2013).
[8] J. D. Denlinger, J. W. Allen, J.-S. Kang, K. Sun, J.-W. Kim, J. H. Shim, B. I. Min, D.-J. Kim, and Z. Fisk, arXiv:1312.6637.
[9] D. J. Kim, J. Xia, and Z. Fisk, Nat. Mater. **13**, 466 (2014).
[10] C.-H. Min, O. Sommer, B. Y. Kang, B. K. Cho, H. Bentmann, and F. Reinert, J. Electron Spectrosc. Relat. Phenom. **199**, 46 (2015).
[11] C.-J. Kang, J. D. Denlinger, J. W. Allen, C.-H. Min, F. Reinert, B. Y. Kang, B. K. Cho, J.-S. Kang, J. H. Shim, and B. I. Min, Phys. Rev. Lett. **116**, 116401 (2016).
[12] H. Yamaoka, P. Thunström, I. Jarrige, K. Shimada, N. Tsujii, M. Arita, H. Iwasawa, H. Hayashi, J. Jiang, T. Habuchi,

D. Hirayama, H. Namatame, M. Taniguchi, U. Murao, S. Hosoya, A. Tamaki, and H. Kitazawa, Phys. Rev. B **85**, 115120 (2012).
[13] Y. V. Kochetkov, V. N. Nikiforov, S. A. Klestov, and A. V. Morozkin, J. Magn. Magn. Mater. **157/158**, 665 (1996).
[14] D. V. Vyalikh, S. Danzenbächer, C. Krellner, K. Kummer, C. Geibel, Y. Kucherenko, C. Laubschat, M. Shi, L. Patthey, R. Follath, and S. L. Molodtsov, J. Electron Spectrosc. Relat. Phenom. **181**, 70 (2010).
[15] S. Patil, A. Generalov, M. Güttler, P. Kushwaha, A. Chikina, K. Kummer, T. C. Rödel, A. F. Santander-Syro, N. Caroca-Canales, C. Geibel, S. Danzenbächer, Y. Kucherenko, C. Laubschat, J. W. Allen, and D. V. Vyalikh, Nat. Commun. **7**, 11029 (2016).
[16] S. Patil, K. Kummer, A. Hannaske, C. Krellner, M. Kuhnt, S. Danzenbächer, C. Laubschat, C. Geibel, and D. V. Vyalikh, JPS Conf. Proc. **3**, 011001 (2014).
[17] R. Ballestracci, C. R. Seances Acad. Sci., Ser. B **282**, 291 (1976).
[18] V. V. Nemoshkalenko and V. N. Antonov, *Computational Methods in Solid State Physics* (Gordon and Breach, Amsterdam, 1998).
[19] V. I. Anisimov, F. Aryasetiawan, and A. I. Lichtenstein, J. Phys. Condens. Matter **9**, 767 (1997).
[20] V. I. Anisimov, J. Zaanen, and O. K. Andersen, Phys. Rev. B **44**, 943 (1991).
[21] A. N. Yaresko, V. N. Antonov, and P. Fulde, Phys. Rev. B **67**, 155103 (2003).
[22] J. K. Lang, Y. Baer, and P. A. Cox, J. Phys. F **11**, 121 (1981).
[23] E.-M. Anton, B. J. Ruck, C. Meyer, F. Natali, H. Warring, F. Wilhelm, A. Rogalev, V. N. Antonov, and H. J. Trodahl, Phys. Rev. B **87**, 134414 (2013).
[24] V. N. Antonov, B. N. Harmon, A. N. Yaresko, and A. P. Shpak, Phys. Rev. B **75**, 184422 (2007).
[25] V. N. Antonov, B. N. Harmon, and A. N. Yaresko, Phys. Rev. B **63**, 205112 (2001).
[26] V. N. Antonov, L. V. Bekenov, and V. P. Antropov, Phys. Rev. B **89**, 165110 (2014).
[27] V. V. Nemoshkalenko, A. E. Krasovskii, V. N. Antonov, V. N. Antonov, U. Fleck, H. Wonn, and P. Ziesche, Phys. Status Solidi B **120**, 283 (1983).
[28] O. K. Andersen, Phys. Rev. B **12**, 3060 (1975).
[29] J. P. Perdew and Y. Wang, Phys. Rev. B **45**, 13244 (1992).
[30] P. E. Blöchl, O. Jepsen, and O. K. Andersen, Phys. Rev. B **49**, 16223 (1994).
[31] K. Kliemt and C. Krellner, J. Cryst. Growth **419**, 37 (2015).
[32] U. Fano, Phys. Rev. **124**, 1866 (1961).
[33] A. Chikina, M. Höppner, S. Seiro, K. Kummer, S. Danzenbächer, S. Patil, A. Generalov, M. Güttler, Yu. Kucherenko, E. V. Chulkov, Y. M. Koroteev, K. Köpernik, C. Geibel, M. Shi, M. Radovic, C. Laubschat, and D. V. Vyalikh, Nat. Commun. **5**, 3171 (2014).
[34] S. Danzenbächer, D. V. Vyalikh, K. Kummer, C. Krellner, M. Holder, M. Höppner, Y. Kucherenko, C. Geibel, M. Shi, L. Patthey, S. L. Molodtsov, and C. Laubschat, Phys. Rev. Lett. **107**, 267601 (2011).
[35] M. Güttler, A. Generalov, M. M. Otrokov, K. Kummer, K. Kliemt, A. Fedorov, A. Chikina, S. Danzenbächer, S. Schulz, E. V. Chulkov, Y. M. Koroteev, N. Caroca-Canales, M. Shi, M. Radovic, C. Geibel, C. Laubschat, P. Dudin, T. K. Kim, M. Hoesch, C. Krellner, and D. V. Vyalikh, Sci. Rep. **6**, 24254 (2016).
[36] F. Gerken, J. Phys. F **13**, 703 (1983).
[37] G. K. Wertheim and G. Crecelius, Phys. Rev. Lett. **40**, 813 (1978).
[38] C. Laubschat, G. Kaindl, W.-D. Schneider, B. Reihl, and N. Mårtensson, Phys. Rev. B **33**, 6675 (1986).
[39] W. Gudat, S. F. Alvarado, and M. Campagna, Solid State Commun. **28**, 943 (1978).
[40] A. Chainani, H. Kumigashira, T. Ito, T. Sato, T. Takahashi, T. Yokoya, T. Higuchi, T. Takeuchi, S. Shin, and N. K. Sato, Phys. Rev. B **65**, 155201 (2002).
[41] J. J. Yeh and I. Lindau, At. Data Nucl. Data Tables **32**, 1 (1985).
[42] Yu. Kucherenko, M. Finken, S. L. Molodtsov, M. Heber, J. Boysen, G. Behr, and C. Laubschat, Phys. Rev. B **66**, 165438 (2002).
[43] S. L. Molodtsov, Yu. Kucherenko, D. V. Vyalikh, G. Behr, A. Starodubov, and C. Laubschat, Phys. Rev. B **68**, 193101 (2003).
[44] R. Hayn, Y. Kucherenko, J. J. Hinarejos, S. L. Molodtsov, and C. Laubschat, Phys. Rev. B **64**, 115106 (2001).
[45] M. Höppner, S. Seiro, A. Chikina, A. Fedorov, M. Güttler, S. Danzenbächer, A. Generalov, K. Kummer, S. Patil, S. L. Molodtsov, Y. Kucherenko, C. Geibel, V. N. Strocov, M. Shi, M. Radovic, T. Schmitt, C. Laubschat, and D. V. Vyalikh, Nat. Commun. **4**, 1646 (2013).
[46] K. Kummer, Yu. Kucherenko, S. Danzenbächer, C. Krellner, C. Geibel, M. G. Holder, L. V. Bekenov, T. Muro, Y. Kato, T. Kinoshita, S. Huotari, L. Simonelli, S. L. Molodtsov, C. Laubschat, and D. V. Vyalikh, Phys. Rev. B **84**, 245114 (2011).
[47] B. Johansson, Phys. Rev. B **20**, 1315 (1979).
[48] A. R. Miedema, J. Less-Common Met. **32**, 117 (1973); A. R. Miedema, F. R. de Boer, and P. F. de Chatel, J. Phys. F **3**, 1558 (1973).
[49] S. Danzenbächer, Y. Kucherenko, D. V. Vyalikh, M. Holder, C. Laubschat, A. N. Yaresko, C. Krellner, Z. Hossain, C. Geibel, X. J. Zhou, W. L. Yang, N. Mannella, Z. Hussain, Z.-X. Shen, M. Shi, L. Patthey, and S. L. Molodtsov, Phys. Rev. B **75**, 045109 (2007).
[50] V. Zlatic and J. K. Freericks, Acta Phys. Pol. B **32**, 3253 (2001).
[51] O. Gunnarsson and K. Schönhammer, Phys. Rev. B **31**, 4815 (1985).
[52] Y. Kucherenko (unpublished).
[53] S. Seiro and C. Geibel, J. Phys. Condens. Matter **23**, 375601 (2011); V. Guritanu, S. Seiro, J. Sichelschmidt, N. Caroca-Canales, T. Iizuka, S. Kimura, C. Geibel, and F. Steglich, Phys. Rev. Lett. **109**, 247207 (2012).